Journal of Atmospheric and Terrestrial Physics, Vol. 53, No. 6/7, pp. 599–618, 1991.
Printed in Great Britain.

0021–9169/91 $3.00+ .00
Pergamon Press plc

F-region seasonal behavior as measured by the MU radar

S. FUKAO,* W. L. OLIVER,*‡ Y. ONISHI,* T. TAKAMI,† T. SATO,† T. TSUDA,*
M. YAMAMOTO* and S. KATO*

* Radio Atmospheric Science Center, Kyoto University, Uji, Kyoto 611, Japan;
† Department of Electrical Engineering, Kyoto University, Yoshida, Kyoto 606, Japan;
‡ Department of Electrical, Computer and Systems Engineering, Boston University, Boston, MA 02215, U.S.A.

(*Received in final form* 12 *November* 1990)

Abstract—We present MU radar ionospheric incoherent scatter results from the period December 1986 to August 1988. We extend our previous 3-month model of the ion vector velocity to a full year and determine seasonal variations. We also present solstitial and equinoctial patterns of electron-density and plasma-temperature behavior. Compared with our previous 3-month model, the full-year velocity model is largely diurnal in nature, the higher harmonic being very variable and tending to average out as noise over a long period. The seasonal behavior of the electron density may be explained largely in terms of the behaviors of the neutral composition and of the timing of the diurnal change of direction of the neutral wind with respect to the time of sunset. According to the neutral composition a high-altitude O^+ layer and a low-altitude molecular-ion layer compete for density predominance. The molecular-ion layer often becomes stronger during summer, and also during times of strong magnetic disturbance. The mean equinox daytime *F*-region electron and ion temperatures (T_e and T_i), and particularly their ratio ($T_r = T_e/T_i$), is controlled largely by the electron density, with other specific time-of-day effects. At night $T_r = 1$, and at sunrise $T_r > 1$ at all *F*-region altitudes measured. During midday we have two cases. For a peak *F*-layer density of about 10^6 cm^{-3} or greater, $T_r > 1$ below 300 km altitude and $T_r = 1$ above 300 km altitude; for lower electron densities $T_r > 1$ at all *F*-region altitudes. Near sunset T_r generally increases as the electron density decreases while photoionization is continuing.

1. INTRODUCTION

The Japanese Middle and Upper atmosphere (MU) radar is the newest of the large atmospheric radars capable of detecting the incoherent scatter (IS) from the free electrons in the ionosphere. This radar system has been described by FUKAO *et al.* (1985a, b). IS observations began in December 1985. SATO *et al.* (1989) have discussed the capability of the MU radar and the techniques used for IS observations. OLIVER *et al.* (1988a) have reported on early *F*-region electrodynamics observations with the MU radar, including the development of an ionospheric electric-field model for the MU radar location, the identification of apparent *F*-region dynamo processes, and the report of unusual wavelike behavior in the ionospheric drifts during the GITCAD campaign of January 1987. OLIVER *et al.* (1988b) have discussed the MU radar IS observations during the large magnetic storm of 6–8 February 1986, during which a large-scale gravity wave was observed to pass from north to south in response to the onset of auroral activity. SARYO *et al.* (1989a, b) have reported MU radar measurements of ion drift and its relation with geomagnetic field variations and of the electron density midday bite-out phenomenon. In the current paper we extend previous results from a larger base of MU radar IS data, reporting for the first time the seasonal variations observed in the ionospheric drifts and density and also the behavior of the ionospheric temperatures.

2. THE MU RADAR

FUKAO *et al.* (1985a, b) have discussed the MU radar system and SATO *et al.* (1989) have discussed its sensitivity for IS measurements. We refer the readers to these papers for detailed information on the MU radar. Here we give only those details having particular pertinence to the data presented in this paper. Table 1 lists several of the basic characteristics of the MU radar.

The MU radar is a monostatic radar with an active phased-array system. The antenna is a circular array of 475 crossed yagi elements having a total diameter of 103 m. Each antenna element is connected to a separate low-power transmit–receive module which can be driven coherently with low-level pulses. Because all of the phase shifting and signal division/recombination is carried out at low power, the antenna may be phased to observe in different directions on a pulse-by-pulse basis, or up to a maximum

Table 1. Basic parameters of the MU radar

Parameter	Value
Location	Shigaraki, Shiga, Japan (34.85°N, 136.10°E)
Geomagnetic parameters	Field strength: 0.0402 mT
(300 km altitude)	Declination: 5.7°W
(IGRF 1985)	Dip angle: 48.3°
	Dip latitude: 29.3°
Operational frequency	46.5 MHz
Antenna	Circular array of 475 crossed Yagis
Aperture	8330 m^2
Steerability	0–30° off-zenith, 5° azimuth steps
Partitioning	25 groups of 19 elements each, each separately driveable
Transmitter	475 solid-state amplifiers (one for each antenna element)
	2.4 kW peak (120 W average) power each
Peak power	1 MW maximum
Average power	50 kW maximum
Pulse length	1–512 μs
IPP	0.4–65 ms

of 2500 times per second. This is a major advantage of the MU radar: its effective capability to observe in multiple directions simultaneously. This allows vector velocity measurements to be made without the possibility of velocity changes occurring between pointing positions.

The major detriment for IS operation with the MU radar is the high system noise temperature of about 10,000 K. This is unavoidable galactic background noise encountered at the MU radar operating frequency. Its effect is to degrade the signal-to-noise ratio achievable and to render the MU radar considerably less sensitive than most of the other routinely operating IS radars in the world. Nevertheless, SATO *et al.* (1989) have calculated that for a long-pulse (500 μs) power measurement signal-to-noise values in excess of unity are achievable with the MU radar, such that it can perform essentially as well as any other IS radar for such a measurement. On the other hand, for the very important spectral measurement, with its requirement for the transmission of a waveform of shorter pulses, it was found that the achievable signal-to-noise ratio often drops in practice to only a few per cent, such that long integration times are required to achieve acceptable statistical accuracy.

3. THE DATA

As discussed by SATO *et al.* (1989), different MU radar experiments are used for different measurable quantities. All experiments normally use four beam positions, magnetic north, east, west, and south, all at 20° zenith angle.

Power profile measurements, from which the electron density profile may be estimated, are generally made with a 7-bit Barker-coded pulse having a 64-μs subpulse width, or 9.6-km range resolution. The received power profile is corrected for range dependence and normalized according to *F*-layer peak density information obtained with an on-site ionosonde to produce the electron density profile. A time resolution of 4 min is normally achieved with this experiment.

Plasma drift velocity is measured with a 2-pulse experiment, consisting of two 256-μs pulses separated by a 256-μs gap, yielding a range resolution of 38 km. This provides a measurement of one lag on the signal autocorrelation function, at 512 μs, from which the correlation phase or, equivalently, the plasma drift, may be computed. A time resolution of 45 min is normally achieved with this experiment.

Temperature measurements require a detailed definition of the shape of the signal autocorrelation function, and for this purpose a 4-pulse scheme, providing 6 points on the correlation function, is used. This uses a 96-μs subpulse length (14.4-km range resolution). A time resolution of 45 min is also normally achieved with this experiment. The drift velocity may also be obtained from the 4-pulse measurements, but its accuracy is much inferior to that of the 2-pulse experiment. A typical MU radar experiment is comprised of repeated 1-h data cycles with each cycle consisting of a 15-min power-profile measurement alternated with either a 2-pulse velocity measurement or a 4-pulse temperature measurement. Data are recorded on magnetic tape every few seconds, but the results are generally integrated to the full 15- or 45-min duration before analysis.

4. STATISTICAL ERRORS

SATO *et al.* (1989) presented detailed simulations estimating the errors expected in the physical parameters derived from the various types of MU radar experiments for varying ionospheric conditions. We have had the opportunity to verify these predictions through use of a special experiment. Most MU radar IS experiments rotate continuously among four beam positions. Due to a hardware failure, this rotation did not take place for certain particular experiments during the period September 1987–August 1988, and all data were obtained in one position. Thus for each 1-h integration period during these experiments four independent but simultaneous results were obtained in the same pointing direction, and we have used these as a statistical population from which we could compute an experimental estimate of the errors in the physical parameters. The comparison between the simulated and measured errors are shown in Fig. 1a–e. Here we have sorted and averaged all the measurements according to the signal-to-noise ratio S/N. Each of these figures shows the error vs S/N and the number of observations available vs S/N. The set of three closely spaced lines on each figure are the theoretical results derived by SATO *et al.* (1989) for different ionospheric conditions, as explained in the figure captions. These theoretical results represent the case for which both T_e and T_i are determined from a fit of theoretical spectrum shapes to the data. The daytime results for T_i and T_e (Fig. 1b, d) match the expectations well. At night T_r is assumed to be unity and only a single temperature is determined. This results in the apparent improvement of the data over expectations in Fig. 1a. Although the T_i and T_e errors are only weakly dependent upon T_i, the T_r error does have a substantial dependence on T_i, arising from a large anti-correlation between the T_e and T_i errors. The fact that the measured T_r errors in Fig. 1c are less than the simulated ones for low signal-to-noise values probably results from the fact that these low signal-to-noise values correspond to the higher altitudes from which the signal strength is relatively weak but at which T_i was verified to be substantially greater than 1000 K during the day of measurement. For the velocity errors of Fig. 1e very low uncertainties are predicted for the higher S/N values. We expect that these accuracies are not achieved in practice owing to residual signal contamination effects (meteor echoes, interference, d.c. level subtraction, etc.); we do correct our data for these sources of error [see SATO *et al.* (1989)], but their imperfect removal becomes relatively more important at low levels of random statistical uncertainty.

It might be useful to characterize here the errors expected from such MU radar experiments for this level of the solar cycle. We will generally characterize these errors at the most common signal-to-noise ratios

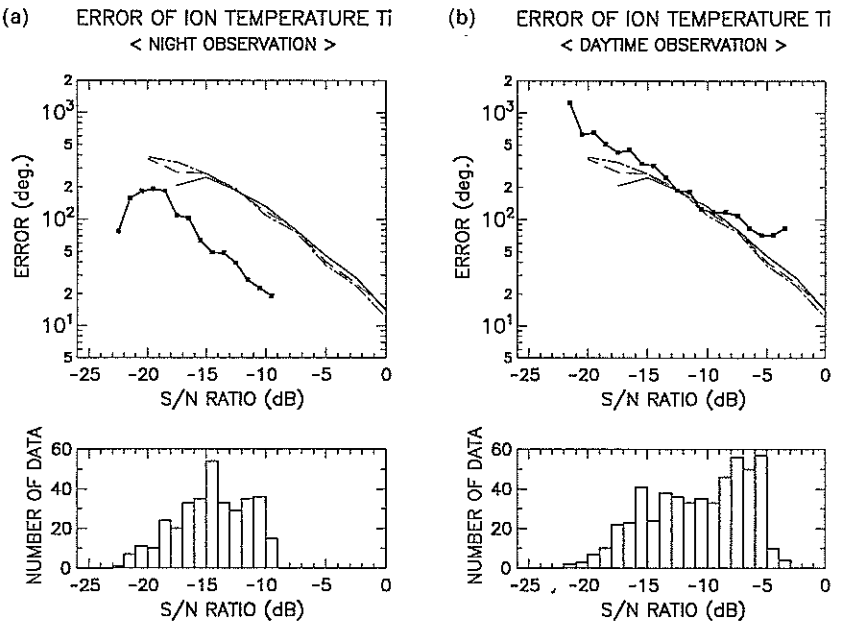

Fig. 1 (a) and (b).

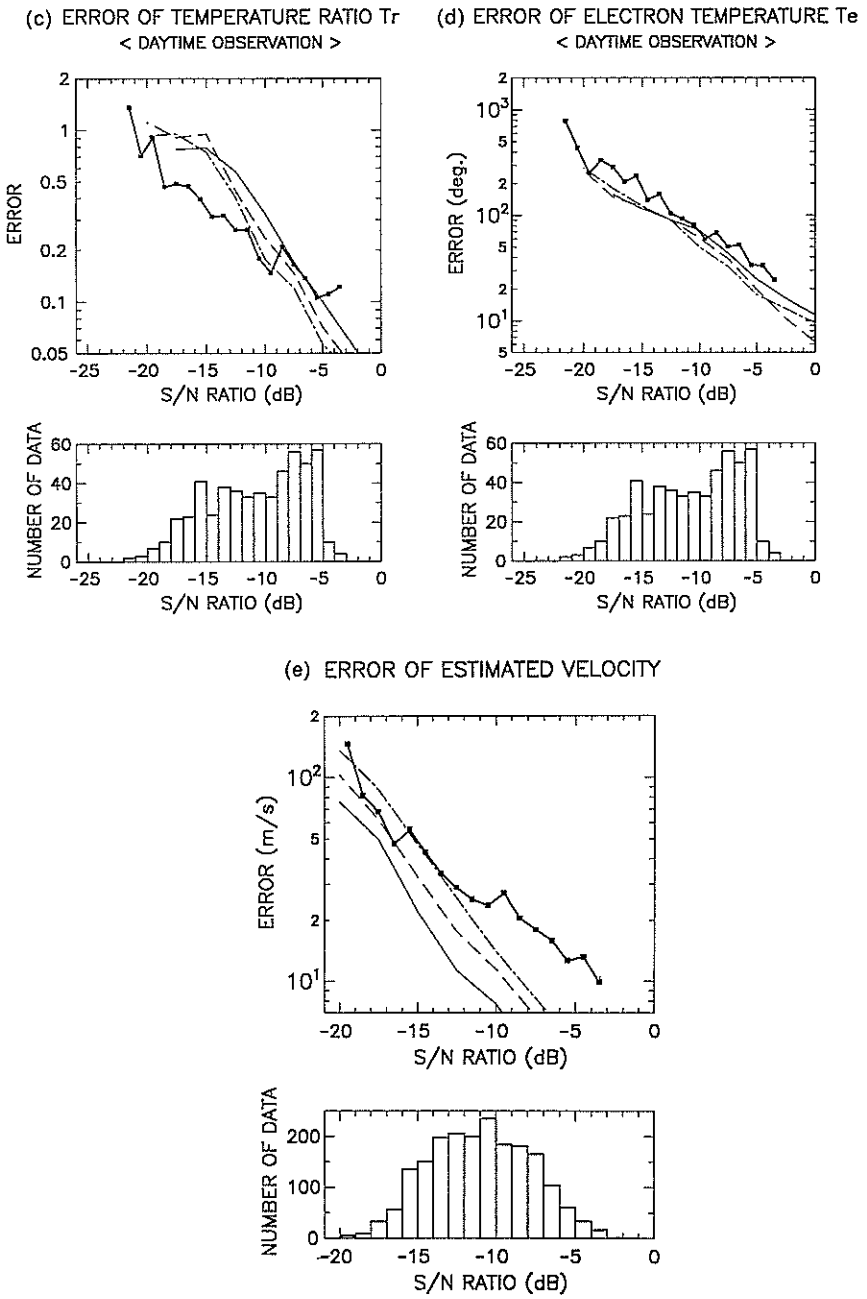

Fig. 1. Comparison of measured and simulated statistical errors in the determination of the physical quantities from MU radar experiments as a function of signal-to-noise ratio S/N: (a) nighttime T_i, (b) daytime T_i, (c) daytime $T_r = T_e/T_i$, (d) daytime T_e, (e) line-of-sight velocity. The measurements are the symbols connected by straight lines. The simulated errors are given for three cases of the ionospheric condition. For (a), (b), (c), and (d) these represent $T_i = 700$ K (solid line), $T_i = 800$ K (long-dash line), and $T_i = 900$ K (long/short-dash line), all for $T_r = 1$. For (e) these represent $T_r = 1$ (solid line), $T_r = 2$ (long-dash line), $T_r = 3$ (long/short-dash line), all for $T_i = 800$ K.

Table 2. Data used for seasonal electron density averages

Season	Year	Start : date and time–End : date and time	Hours	S_a
Summer	1987	1 June 15 LT–5 June 15 LT	96	77
Fall	1987	21 September 12 LT–22 September 16 LT	28	82
		19 October 12 LT–21 October 7 LT	43	96
Winter	1987	24 November 14 LT–26 November 11 LT	45	105
		21 December 12 LT–23 December 11 LT	47	88
Spring	1988	14 March 8 LT–17 March 23 LT	87	113
		19 March 0 LT–22 March 7 LT	79	117

S_a is the 10.7-cm solar flux value.

experienced, and these will generally refer to the main F_2-layer rather than very high or low altitudes of low ionospheric density. At night, when we can assume $T_e = T_i$, the expected temperature errors are in the range 20–200 K, with 50 K being most common. During the day, when both T_e and T_i must be determined from the data, we may expect T_i, T_e, and T_r errors of 70, 30, and 0.1 K, respectively, near the F_2-peak. At altitudes near 500 km, however, these values may range up to 1000 K for the temperatures and up to unity for T_r. The velocity errors at the F_2-peak may be expected to be about 20 m/s. At high altitudes they increase toward 100 m/s.

We should emphasize that these are the expected errors in each pointing position. Should we combine all four positions (as we may wish to do for the scalar quantities), we would reduce these errors by a factor of two.

5. ELECTRON DENSITY RESULTS

We present here contour plots of electron density N_e vs altitude and local time to represent the patterns seen at the solstices and at the equinoxes by the MU radar. Each plot is an average over several days of measurements. The dates used for these averages are given in Table 2. The contour plots are given in Fig. 2a–d. The whited areas on the graphs hide regions of spurious data related to poor *F*-region signal strength; these areas tended to accumulate during the averaging process. Also, the post-midnight/pre-dawn regions of enhanced N_e in the *E*-region, as displayed on these figures, probably represent the effect of unsuccessfully rejected meteor echoes or coherent-echo returns from field-aligned irregularities imbedded in sporadic-*E* layers entering through the antenna sidelobes.

The summer pattern seems complicated but portrays several features common to that season. There are many local maxima on this map, and their appearance is to some degree affected by the choice of contour levels. The primary features, however, are that the peak of the layer is often broad and flat during the daytime and that the density remains at relatively high values until well after sunset and remains fairly high throughout the night. These features are explicable in terms of the summer patterns of neutral composition and meridional wind direction. Figure 3a gives nominal noontime winter and summer N_e profile shapes as determined by the study of TANAKA and HIRAO (1972) while Fig. 3b gives representative summer and winter profiles measured by the MU radar. These two figures show similar changes in profile shape with season, and the reasons for these changes are explained by Tanaka and Hirao. Tanaka and Hirao adopted a neutral atmosphere and incident solar ionizing flux and proceeded to compute the densities and temperatures of the various charged-particle species produced. Their summer and winter cases correspond to noon at 35°N latitude over Japan for the months of January and August 1971. Inputs to their model were chosen to yield electron density behavior approximating monthly median ionosonde results for this time and location. The neutral atomic oxygen density was made three times as large in winter as in summer at the base of the thermosphere but the neutral molecular densities and temperature at this altitude were held constant. The model computed, as expected, a higher neutral temperature in summer, and the neutral densities above the base of the thermosphere obeyed the barometric law. In looking at seasonal variations in the electron density at higher altitudes, we must consider the seasonal variation in atomic oxygen imposed at the base of the thermosphere and the increased densities of the neutrals in summer owing to the increase in temperature in summer. In the winter, as compared with summer, the neutral atomic oxygen density is high and the neutral molecular oxygen and nitrogen densities are low in the *F*-region. This leads, through normal photochemical processes, to a high O^+ density in the *F*-region (near 250 km altitude in Fig. 3) and a low molecular-ion density (O_2^+ and NO^+) in the *E*- or lower F_1-region

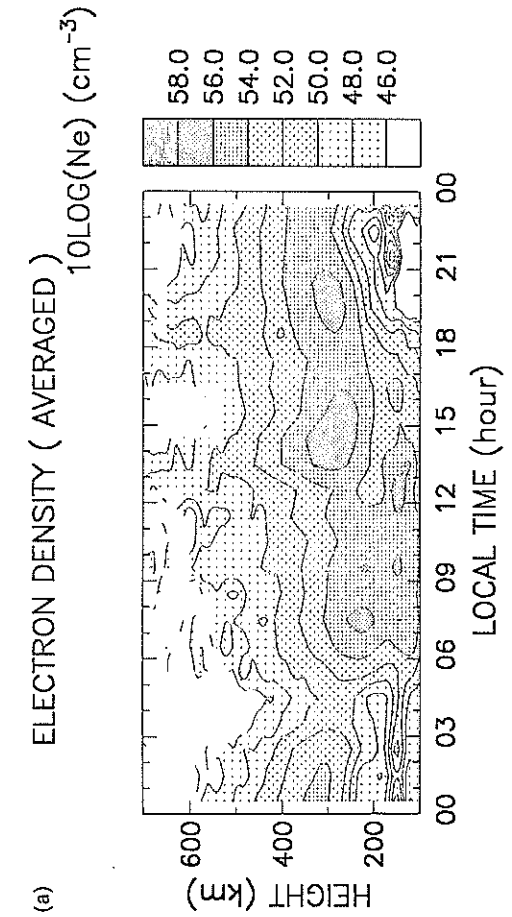
(a)
ELECTRON DENSITY (AVERAGED)
10LOG(Ne) (cm-3)
58.0
56.0
54.0
52.0
50.0
48.0
46.0
HEIGHT (km)
600
400
200
00 03 06 09 12 15 18 21 00
LOCAL TIME (hour)

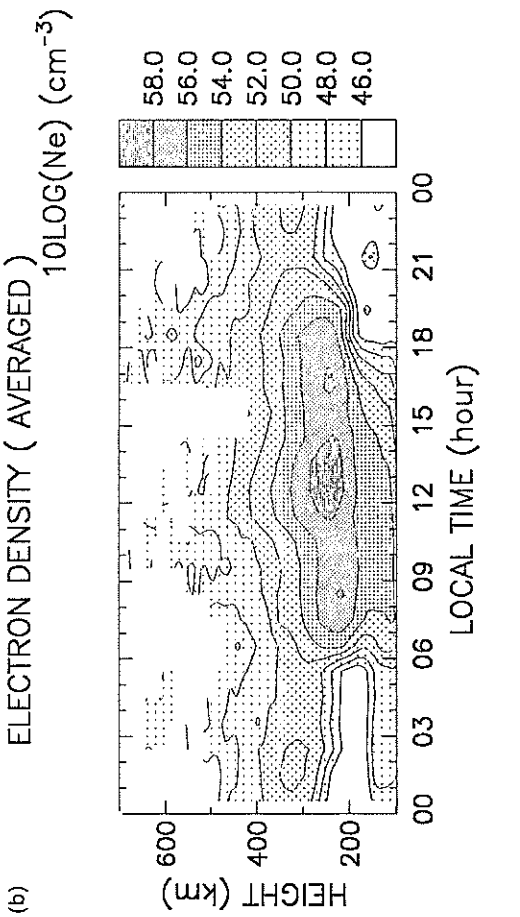
(b)
ELECTRON DENSITY (AVERAGED)
10LOG(Ne) (cm-3)
58.0
56.0
54.0
52.0
50.0
48.0
46.0
HEIGHT (km)
600
400
200
00 03 06 09 12 15 18 21 00
LOCAL TIME (hour)

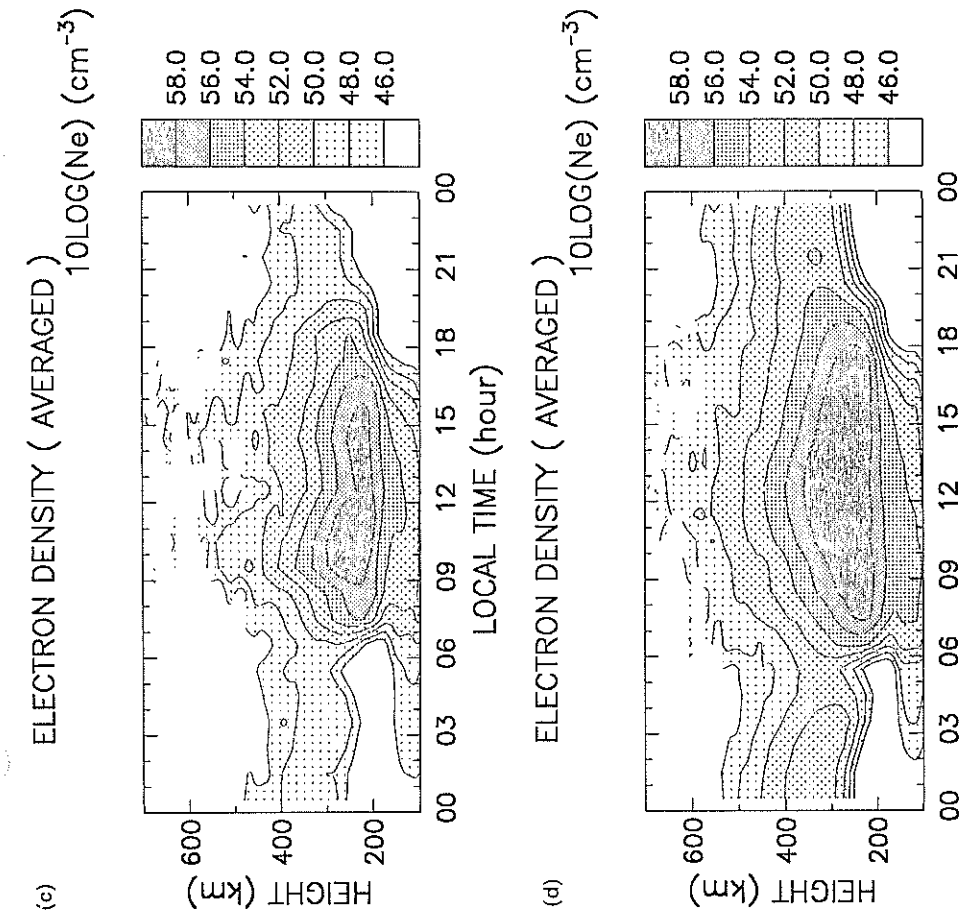

Fig. 2. The average seasonal patterns of electron density as determined from selected seasonal data : (a) summer pattern, averaged from the 1–5 June 1987 data, (b) fall pattern, averaged from the 21–22 September and 19–21 October 1987 data, (c) winter pattern, averaged from the 24–26 November and 21–23 December 1987 data, and (d) spring pattern, averaged from the 14–17 and 19–22 March 1988 data.

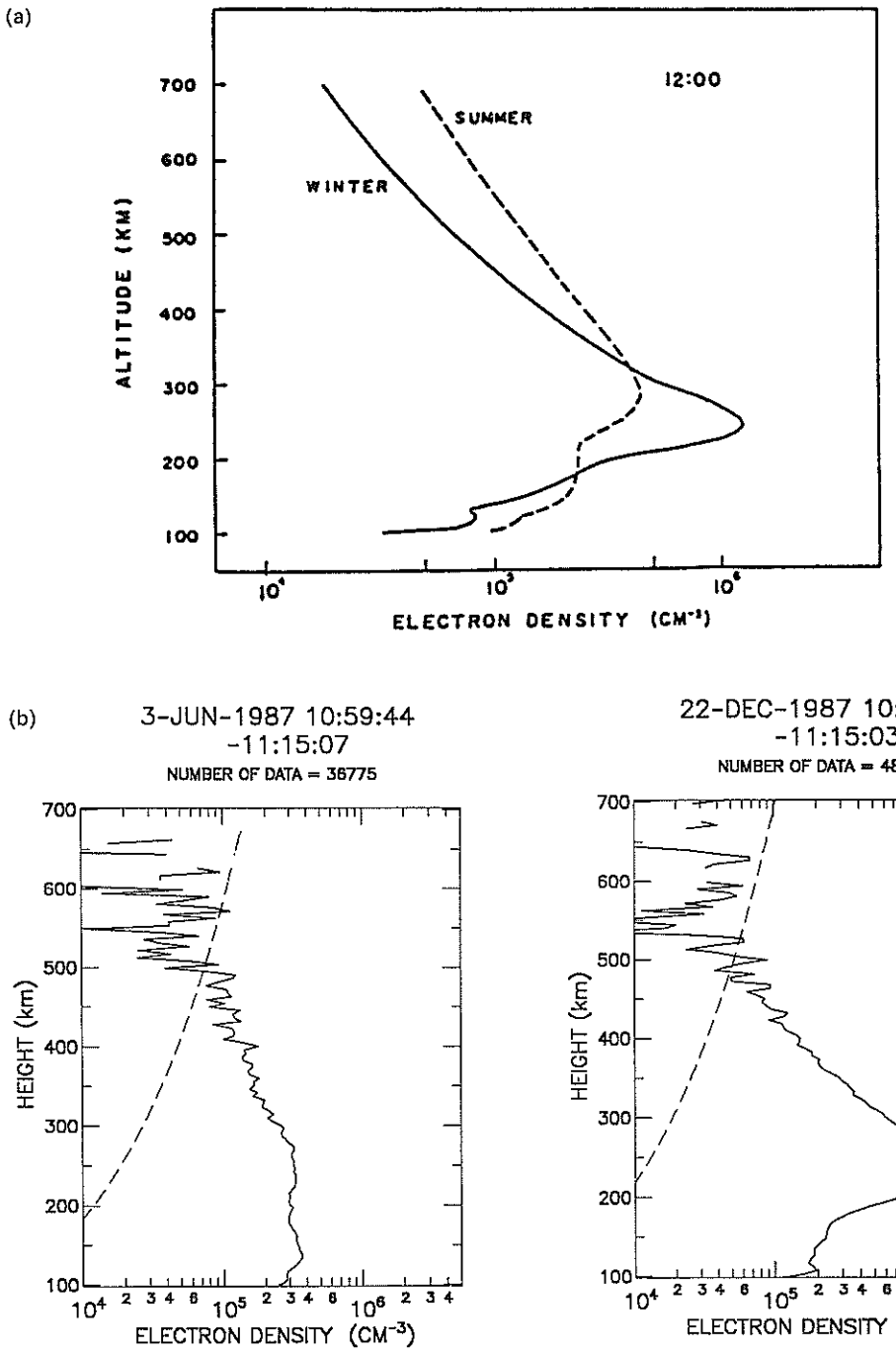
(a)
12:00
SUMMER
WINTER
ALTITUDE (KM)
700
600
500
400
300
200
100
10^4
10^5
10^6
ELECTRON DENSITY (CM^{-3})
(b)
3-JUN-1987 10:59:44
-11:15:07
NUMBER OF DATA = 36775
22-DEC-1987 10:59:42
-11:15:03
NUMBER OF DATA = 48625
HEIGHT (km)
ELECTRON DENSITY (CM^{-3})

Fig. 3 (a) and (b).

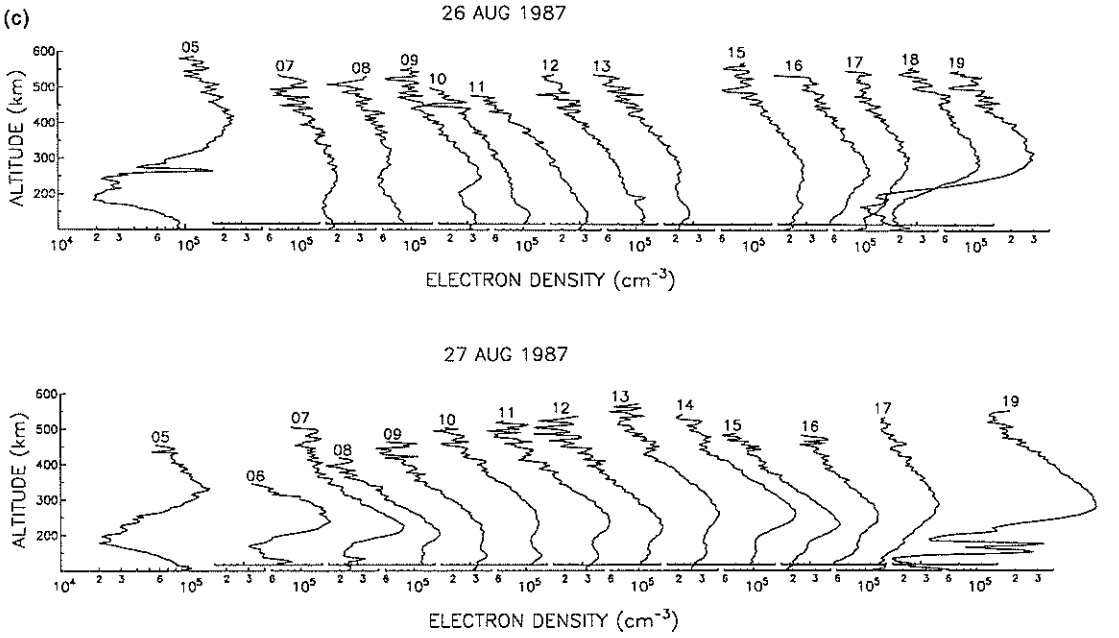

Fig. 3. Representative summer and winter electron density profile shapes as determined from (a) the study of TANAKA and HIRAO (1972), and from (b) MU radar solstice measurements, and (c) a sequence of N_e altitude profiles measured on 26–27 August 1987, showing the competition between the upper and lower layers for dominance.

(near 150 km in Fig. 3). The O^+ layer is dominant by far in the winter. In the summer the composition situation is reversed, and the O^+ and molecular-ion layers attain more comparable peak densities. This seasonal difference in the magnitude of the O^+ layer peak density is the so-called winter anomaly of the F_2-layer. For some ionospheric conditions, the neutral composition is such that the molecular-ion layer peak density can exceed the O^+ layer peak density. These composition conditions are often achieved under magnetically disturbed conditions, when the O^+ density is greatly depleted, and it is at these times that the so-called 'G' condition on ionograms is seen. In the topside ionosphere, the higher summer density is caused by the higher summer temperature, and hence the larger diffusive scale height. In Fig. 2a the ionosphere is particularly thick from 0600 to 1200 LT, with little change in density from some 100–300 km altitude. This may be explained by the existence of O^+ and molecular-ion layers, near 250 and 150 km altitude, respectively, of similar peak density. In the afternoon the upper layer density is enhanced while the lower layer density is diminished. This could be explained simply by a decrease in the neutral N_2 and/or O_2 densities in the thermosphere. Such an occurrence would serve both to increase the O^+ layer density (through a decreased loss rate) and decrease the molecular-ion layer density (through a decreased production rate).

As further emphasis of this point, we show in Fig. 3c a series of electron density profile shapes measured on 26–27 August 1987. These profile shapes show clearly the evolutions of the O^+ layer at 200–300 km altitude and of the molecular-ion layer below 150 km altitude and the competition between these layers for dominance. A magnetic storm was in progress when these measurements were begun, and this served to reduce the O^+ layer density strongly on 26 August while the densities on 27 August were at more nearly normal levels.

The increase of the *F*-layer peak density between 1800 and 2100 LT in Fig. 2 probably represents a dynamical effect of meridional winds. We plan a separate study of the winds from MU radar data to help confirm this assertion, but at this time we will simply put forward a qualitative explanation. To first order, in the *F*-region, the winds blow basically away from the sub-solar point in great circles around the Earth. Thus the *F*-region meridional winds blow poleward by day, forcing the *F*-laying downward along the geomagnetic field lines, while they blow equatorward by night, forcing the *F*-layer upward. Because the summer day is long, these winds generally change from poleward to equatorward, lifting the *F*-layer to

high altitudes, while the Sun is still producing new ionization. This results in a high equilibrium density at a high altitude of low loss frequency for these O^+ ions. Thus a high evening F-layer density and a slow decay of this density is experienced. Sunset was near 2030 LT during this measurement period, and the aforementioned pattern is clearly evident in the data (Fig. 2a). These patterns of behavior are consistent with the winds effects found in the numerical studies of KOHL and KING (1967) and STROBEL and MCELROY (1970).

The winter pattern (Fig. 2c) shows many features contrasting with the summer pattern. The F-layer is narrow and strong, and the higher O^+ layer dominates the lower molecular-ion layer. The day is short, and thus the winds are still poleward, forcing the F-layer downward, when solar production stops. This leads to a rapid loss of ionization and to low peak densities by the time the winds reverse to the equatorward direction to raise the layer and arrest the rapid loss. The densities remain low all night, but they often reach a minimum residual level. This level must be maintained by a flux of ionization from the overlying plasmasphere. Our velocity measurements at high altitudes are too poor to give direct evidence of these fluxes. The upper altitude of useful density measurement by the MU radar is reduced in winter in accordance with the smaller scale height and density levels in the topside ionosphere.

In the next section we will present the plasma drift velocity results. These will confirm some of our discussion on the wind effects on the summer and winter evening electron density levels, for they show that the plasma drift turns upward along the field line in summer near 1630 LT but in winter near 2130 LT. These times, in correspondence with the times of sunset during summer and winter, lead to the relatively large nighttime densities in summer and relatively small nighttime densities in winter.

The fall and spring patterns show situations intermediate between the summer and winter patterns. The spring densities are actually the largest shown in Fig. 2. We must note, however, that the solar flux was rapidly increasing during the four consecutive seasons shown here, having the values listed in Table 2. The spring solar flux was the highest, and thus we do not feel confident to ascribe the large spring densities to either a seasonal or solar-activity cause.

Our electron density data often show the midday 'bite-out' effect, seen when poleward winds force the ionosphere downward to regions of lower equilibrium density (SARYO *et al.*, 1989b). These patterns are largely smeared out in our seasonal averages, although some hint of this effect may be seen in the summer and winter patterns.

Table 3. Data used for seasonal velocity averages

Year	Start date–End date	Hours	Season
1986	16 December–19 December	64	Winter
1987	27 April–1 May	87	Equinox
	1 June–5 June	96	Summer
	19 October–21 October	45	Equinox
	21 October–23 October	29	Equinox
	17 November–20 November	42	Winter
	24 November–26 November	45	Winter
	17 December–18 December	8	Winter
	21 December–23 December	47	Winter
1988	12 January–14 January	47	Winter
	18 January–21 January	45	Winter
	14 March–17 March	76	Equinox
	13 June–15 June	49	Summer

6. PLASMA DRIFT VELOCITY RESULTS

Table 3 lists the MU radar IS experiments during the period 16 December 1986–15 June 1988 for which the magnetic activity index remained at or below $K_p = 3$. Few experiments corresponded to higher K_p. We have used these data to compute the average plasma drift behavior in the F-region over the MU radar. OLIVER *et al.* (1988a) averaged three months of such data (October–December 1986); our current emphasis is to determine seasonal behaviors and an improved all-year average from an extended data base. Figure 4a–c shows these all-year averages. The data have been sorted into 1-h bins and averaged. The 'error' bars in these figures give the standard deviation of the population in each bin. There are on average some 30 points per bin, so the uncertainties in the average values themselves are about a factor of five smaller. The data have been averaged over the altitude range 199.2–302.9 km to improve statistical quality.

We have fit diurnal harmonics to the data of Fig. 4, and the magnitudes and phases of these components are summarized in the dial plots of Fig. 5a–c. The daily mean value is given on the dial plots as the 'DC' level. Table 4 summarizes the mean values and amplitudes and phases for these harmonic components for the all-year as well as for the seasonal averages to be presented subsequently. Much of our following discussion will relate to the information in Table 4.

We wish to discuss the perpendicular velocities in relation to the electric field model of RICHMOND *et al.* (1980), as reproduced in Fig. 6. Richmond derived his model from incoherent scatter data collected from altitudes of about 300 km in the American and European longitude sectors. Richmond's model covers a range of latitudes, and it is the 30° latitude results

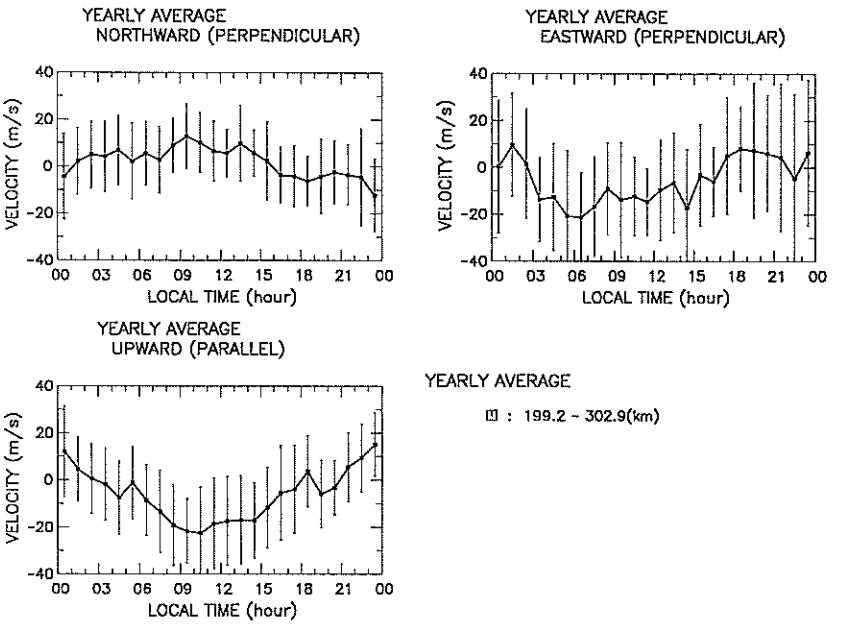

Fig. 4. The all-year average plasma drift velocity determined from the experiments listed in Table 3. The vertical bars represent the standard deviation of the population in each 1-h time bin. These standard deviations must be divided by a factor of about 5 to obtain the uncertainties in these mean values.

Table 4a. All-year average velocity components (in m/s)

Component	$V_{\perp E}$	$V_{\perp N}$	$V_{\parallel up}$
Mean	−5.56	1.95	−5.95
24-h Amplitude	11.25	7.49	14.28
Phase	20:45	9:24	23:13
12-h Amplitude	1.72	1.36	1.18
Phase	10:39	1:55	2:30
8-h Amplitude	5.11	2.03	2.15
Phase	3:03	5:29	7:20

Table 4b. Equinox average velocity components (in m/s)

Component	$V_{\perp E}$	$V_{\perp N}$	$V_{\parallel up}$
Mean	−3.81	0.81	−2.31
24-h Amplitude	10.14	8.56	13.17
Phase	21:49	9:21	23:12
12-h Amplitude	0.83	1.30	2.83
Phase	7:11	11:57	3:55
8-h Amplitude	6.10	3.53	5.18
Phase	2:07	5:50	0:01

Table 4c. Summer average velocity components (in m/s)

Component	$V_{\perp E}$	$V_{\perp N}$	$V_{\parallel up}$
Mean	−9.03	2.48	0.57
24-h Amplitude	12.15	8.49	9.29
Phase	17:50	10:35	22:01
12-h Amplitude	3.94	0.89	1.85
Phase	1:27	7:19	1:32
8-h Amplitude	11.88	2.78	1.93
Phase	3:10	2:37	5:11

Table 4d. Winter average velocity components (in m/s)

Component	$V_{\perp E}$	$V_{\perp N}$	$V_{\parallel up}$
Mean	−3.94	2.41	−14.16
24-h Amplitude	15.10	6.45	19.87
Phase	21:58	8:58	0:22
12-h Amplitude	5.86	2.14	3.13
Phase	9:13	2:00	9:46
8-h Amplitude	0.71	2.06	1.92
Phase	2:29	3:26	5:15

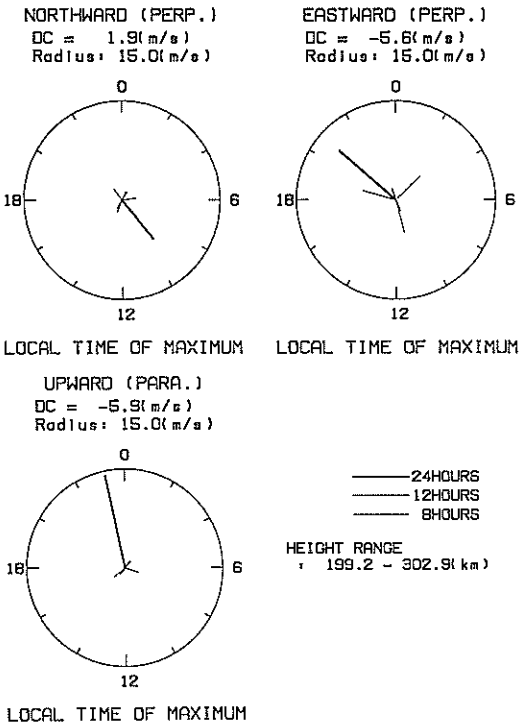

Fig. 5. Dial plots describing the mean and harmonic component fits to the all-year average plasma drift velocity. See Table 4 for tabulated amplitudes and phases.

which closely match the MU radar magnetic latitude. Because the magnetic declination is small for the MU radar location the local time of our data presentation and the magnetic local time of the Richmond model differ by only a small amount.

Richmond's 'upward/poleward' component is equivalent to our 'northward (perpendicular)' component. Our data show a strongly diurnal behavior in this perpendicular-north component while Richmond's model contains an additional strong semidiurnal component. The main discrepancy here concerns a secondary maximum just before midnight. This is present in the model but absent in the data. The MU radar data actually agree better in phase with the lowest latitudes of Richmond's model, where the semidiurnal term is smallest. This difference could be related to the difference in the geomagnetic/geographic relationships between the Asian and American/European sectors. Otherwise, the time of the primary maximum of the data is advanced by about 1 h from, and the amplitude of the daily variation in the data is about one-third smaller than, the model values.

The eastward-perpendicular components of the data and of the model also show excellent phase agreement for the main evening peak velocity, and both show predominantly diurnal components. The model amplitude, however, is twice as large as the amplitude

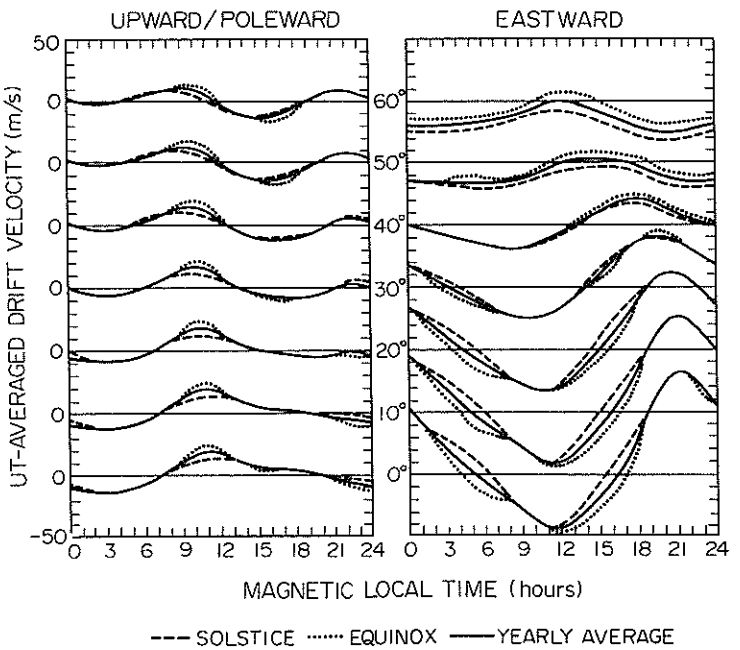

Fig. 6. The perpendicular drift model of RICHMOND *et al.* (1980). The curves at 30° magnetic latitude are those to be compared with the MU radar data.

seen in the MU radar average, and the MU radar data exhibit a substantial terdiurnal component missing from the model. The parallel drift, not included in Richmond's model, is very strongly diurnal, with a peak upward drift occurring close to midnight. The daily mean drifts are small for all of these components.

These comparisons with Richmond's model were also made in the earlier study by OLIVER *et al.* (1988a) from the more limited October–December 1986 data set. The main differences between the previous 3-month and the present 12-month results are as follows. In all cases, the amplitudes of the semidiurnal and terdiurnal components are now reduced, strongly so for the perpendicular components. The diurnal component is the dominant component in the 12-month model whereas its amplitude had been matched or even exceeded by the amplitudes of higher-order harmonics in the perpendicular components in the 3-month model. The amplitudes of the diurnal components are all reduced by a small amount for the 12-month average, but the phases have remained essentially unchanged for the perpendicular-east and parallel components and has changed by less than 2 h for the perpendicular-north component.

All of these comparisons, between our 3-month and 12-month models and Richmond's model, point to a strong stability of the diurnal variation and a strong variability of the higher-order harmonics. RICHMOND *et al.* (1976) have pointed out that almost all of the quiet-day ionospheric currents may be attributed to the combination of an *in-situ*-generated diurnal tide and an upward-propagating semidiurnal tide. The diurnal tide should be stable, owing to the stability of the daily solar illumination causing it, while the electric fields generated by the semidiurnal tide should be variable, owing to the known variability of the winds generating them. It is not surprising, then, that the higher harmonics lack consistency and tend to be averaged out for the longer averaging period.

The strongly diurnal nature of the parallel drift reflects the strong control by the diurnal wind direction. This wind is poleward by day, pushing the ionization down the field lines, and equatorward by night, pushing ionization up the field lines, in agreement with the observed parallel velocity direction. Plasma diffusion also contributes a major component of the parallel velocity. This diffusion velocity is always downward, but is more strongly so below the *F*-layer peak, where gravity and diffusion act downward together, and less strongly so above the peak, where the gradient and gravitational forces oppose. Because the F_2-peak rises by night and falls by day (see Fig. 2), we can say, in a qualitative sense, that we should see, at our constant observing altitude of 250 km, a diffusion velocity contribution which is more strongly downward by night than by day. But this is opposite to the pattern of Fig. 4, so the observed diurnal pattern is not a result of diffusion. The wind and diffusion effects tend to cancel, but the wind effect is the stronger and controls the diurnal pattern seen.

We show in Figs 7–9 the velocity results of Figs 4–5 separated into seasons, with spring and fall combined to a single equinox season. Table 3 gives the experiments placed in each season. We will discuss first the diurnal components of these results, as these seem to be more stable.

For the parallel velocity we see a substantial change in amplitude with season, the winter amplitude being about twice as large as the summer amplitude. Also there is a phase progression, with the maximum downward velocity occurring near 1000 LT in summer and 1220 LT in winter. The equinox results lie intermediate between these solstice values. In addition, a substantial downward mean velocity develops during the winter. Figure 9c shows that this velocity is downward for most of the day, becoming upward for only a short time around midnight. BABCOCK and EVANS (1979) have computed the daily mean meridional wind from six years of data from Millstone Hill. Their results show a northward wind in winter, indicating a downward parallel ion velocity, and a southward wind in summer, indicating an upward ion drift. This would seem to define a large-scale summer-to-winter circulation pattern. While the MU radar results also show the downward parallel drift in winter, no significant daily average velocity is found for the remainder of the year. The location of the MU radar near the sub-solar point in summer and its large distance from the auroral zone could explain these geographical differences in behavior. A detailed study of this effect requires a true computation of the winds from the observed plasma drifts, a study which will be reported separately.

We note here again that the parallel velocity turns upward in summer near 1630 LT but in winter only near 2130 LT. Combined with the times of sunset for summer and winter this causes an enhancement of the summer evening density and a maintenance of the summer nighttime density and the exactly opposite effect in the winter. These patterns are evident in our electron density averages (Fig. 2).

The perpendicular-north velocity is relatively stable with season. The winter amplitude is reduced by about 25% and its phase is rotated 1.6 h earlier with respect to summer. The perpendicular-east velocity (diurnal component) is more variable. The amplitude is weakest at the equinoxes, strongest in winter. The summer phase is 4 h behind the other seasons.

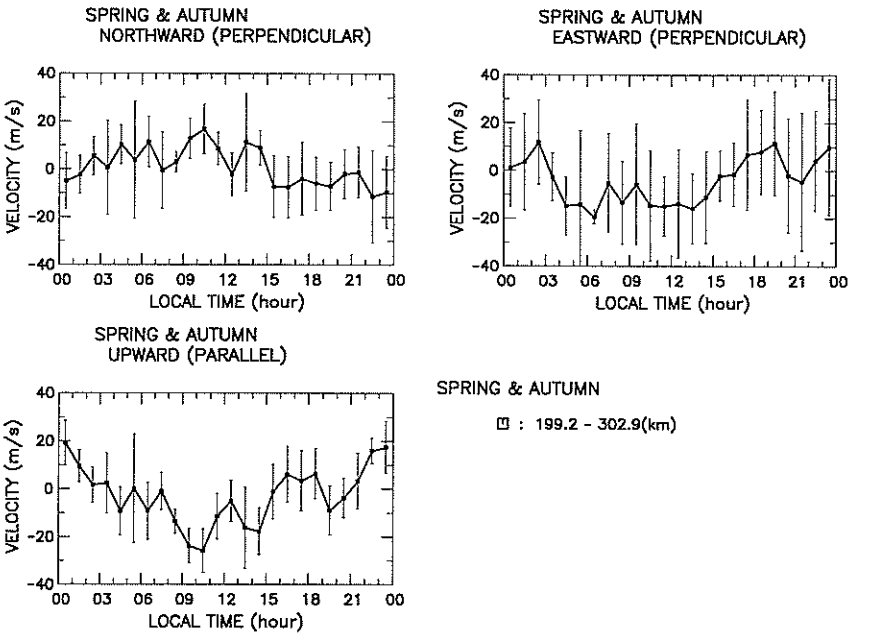

Fig. 7. The equinox average plasma drift velocity. See the captions of Fig. 4 for an explanation of the presentation.

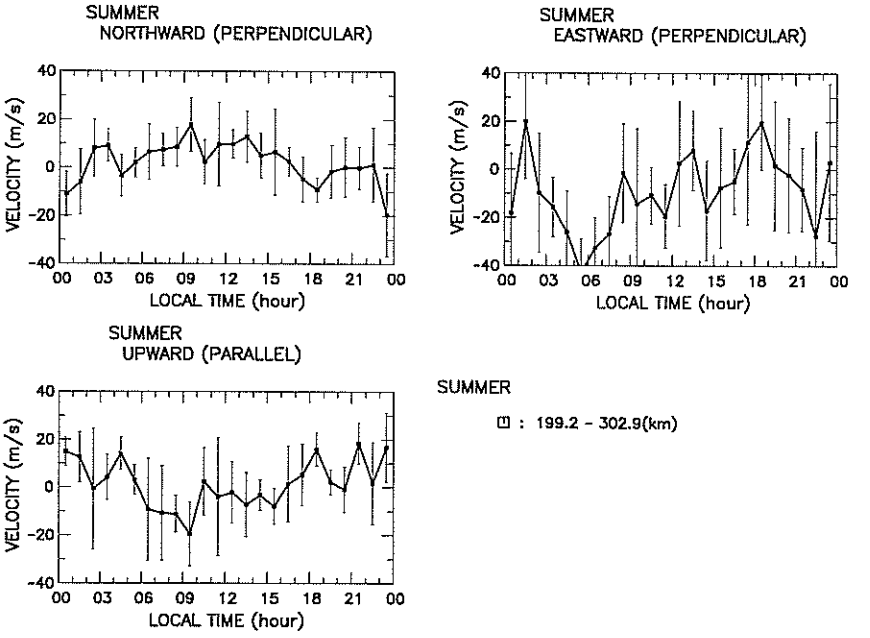

Fig. 8. Same as Fig. 7, for the summer average.

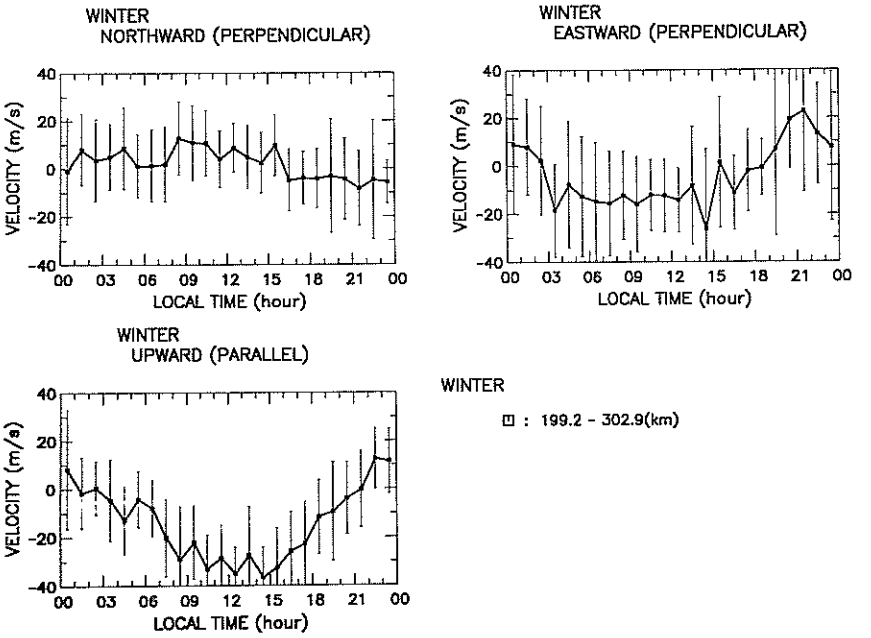

Fig. 9. Same as Fig. 7, for the winter average.

For reasons discussed previously, we do not have faith that the higher harmonic results represent permanent behavior in the ionosphere. Nevertheless, we do note that these harmonics remain small at all seasons for the parallel and perpendicular-north velocities, but that great variability occurs in the perpendicular-east velocity. The terdiurnal term becomes almost as large as the diurnal in summer but vanishes in winter. A relatively large diurnal mean value also appears in summer for this component.

The velocities that we have discussed move the ionosphere upward or downward according to the net vertical motion produced by the winds and the electric fields. We observe frequent cases of *F*-region dynamo behavior at night when wind motions generate feedback electric fields that cancel the original vertical motion caused by the winds, such that the ionosphere moves horizontally with the wind. We also sometimes observe the reverse-cause effect in the daytime, when plasma motions, caused by *E*-region dynamo fields, drag neutral winds which cancel the original vertical plasma motion caused by the fields. We refer the reader to OLIVER *et al.* (1988a) for a fuller discussion of these effects.

7. PLASMA TEMPERATURE RESULTS

SATO *et al.* (1989) showed examples of the electron and ion temperatures measured throughout the 29-h experiment of 5–6 November 1986. These are typical of the results obtained by the MU radar. We wish here to illustrate how these temperatures vary under differing conditions. Figure 10 shows the N_e, T_e, T_i, and $T_r = T_e/T_i$ measurements made throughout the day on 20 March 1988. Error bars here are estimated from the measured signal-to-noise according to the simulations of SATO *et al.* (1989). There is a sunrise effect, when the sudden solar heating is applied to a low nighttime plasma density, creating high T_e during the period of ionization build-up. The electrons heat the ions during this period. T_e then decreases toward midday as N_e increases. This midday decrease in T_e has been observed at Millstone Hill, Arecibo, and Jicamarca (e.g. EVANS, 1971). During the main part of the day, T_r decreases with increasing altitude from 200 to 350 km altitude. To emphasize this point further, we have averaged the T_e, T_i, and T_r profiles over the daytime period 1000–1600 LT to show their profile shapes. The result is shown in Fig. 11. T_r is seen to be essentially unity above 300 km altitude. T_r increases at the higher altitudes toward late afternoon, then falls to unity quickly after sunset as heating ceases. T_r is assumed to be unity well before sunrise and well after sunset in our data analyses, as indicated on these figures. To illustrate this further, we show the altitude profiles of these temperatures and of the electron density for the post-sunrise, midday, and late-afternoon cases in Fig. 12a–c. What maintains T_e at

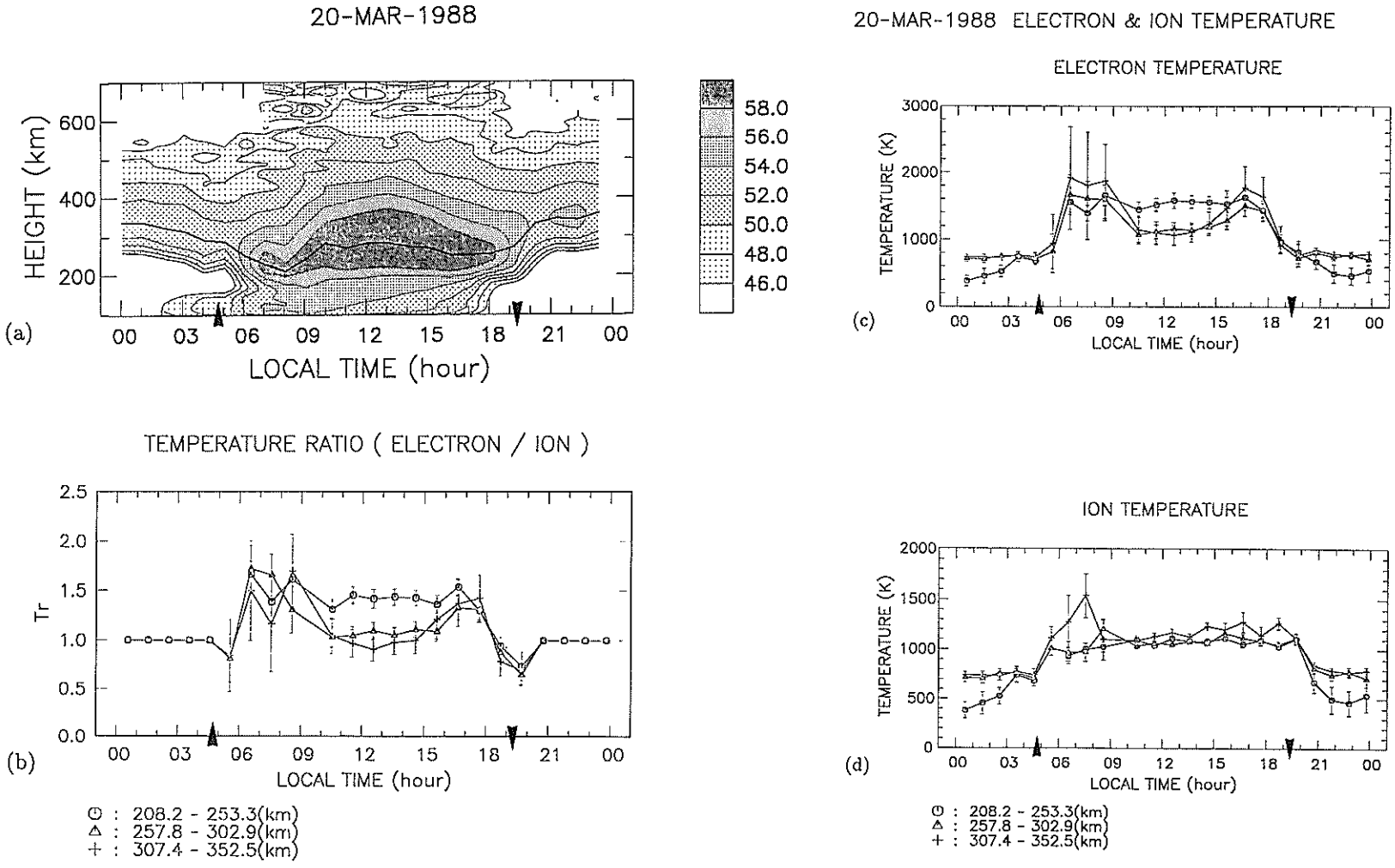

Fig. 10. N_e, $T_r = T_e/T_i$, T_e, and T_i measured on 20 March 1988. Arrows mark the times of sunrise and sunset.

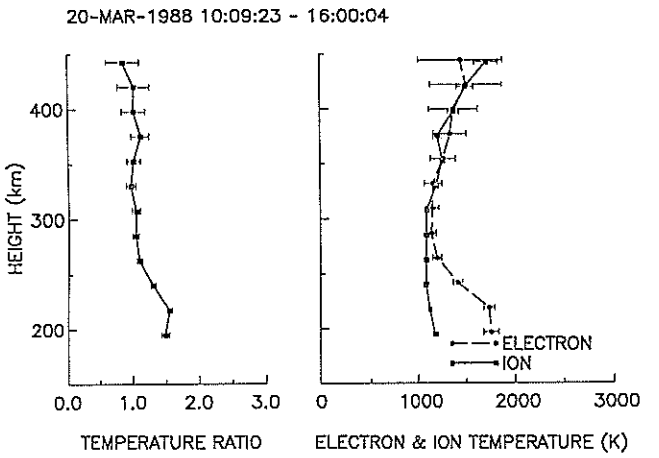

Fig. 11. T_e, T_i, and $T_r = T_e/T_i$ averaged over 1000–1600 LT on 20 March 1988.

the T_i level during the middle of the day is the rapid cooling caused by the high ion density. The midday density profile shows both a higher peak density and a higher peak altitude in comparison with the late-afternoon case, so that the topside densities, above 300 km altitude, are much higher for the midday case, causing strong cooling of the plasma. The low morning densities cannot maintain a low T_e level. In contrast with this, we show another equinox result, from 21 September 1987, in Fig. 12d. This midday measurement shows T_e maintained well above T_i. The difference here is the much lower electron density of the ionosphere for the September case. The solar 10.7-cm flux indices were 83 and 116 units, respectively, for the September and March cases. This is the pattern that we see with the MU radar, of a T_r value which varies inversely with the electron density due to cooling processes. This pattern is routinely observed on short time scales also (i.e. during the course of a day).

8. CONCLUDING REMARKS

We have presented MU radar ionospheric incoherent scatter results from the period December 1986 to August 1988 in an extension of our previous analysis of the October–December 1986 period. In the previous paper we presented the 3-month average behavior of the ion vector velocity. In this paper we have extended that model to a full year, determining seasonal variations also. We have also presented solstitial and equinoctial patterns of electron-density and plasma-temperature behavior. Concerning the new full-year velocity model, we noted that all velocity components are largely diurnal in nature, and that, compared with our previous 3-month model, the higher harmonics are much reduced in amplitude. The diurnal component seems to be the primary permanent component of behavior while the higher harmonics seem to be variable from experiment to experiment and hence average out as random noise over a long period, though they may have substantial importance on a given day. The seasonal behavior of the electron density may be explained largely in terms of the behaviors of the neutral composition and of the timing of the diurnal change of direction of the neutral wind with respect to the time of sunset. According to the neutral composition a high-altitude O^+ layer and a low-altitude molecular-ion layer compete for density predominance. The molecular-ion layer often becomes stronger during summer, and also during times of strong magnetic disturbance of the neutral composition. The mean equinox daytime F-region electron and ion temperature (T_e and T_i), and particularly their ratio ($T_r = T_e/T_i$), is controlled largely by the electron density, with other specific time-of-day effects. At night $T_r = 1$, and at sunrise $T_r > 1$ at all F-region altitudes measured. During midday we have two cases. For a peak F-layer density of about 10^6 cm^{-3} or greater, $T_r > 1$ below 300 km altitude and $T_r = 1$ above 300 km altitude; for lower electron densities $T_r > 1$ at all F-region altitudes. Near sunset T_r generally increases as the electron density increases if photoionization is continuing.

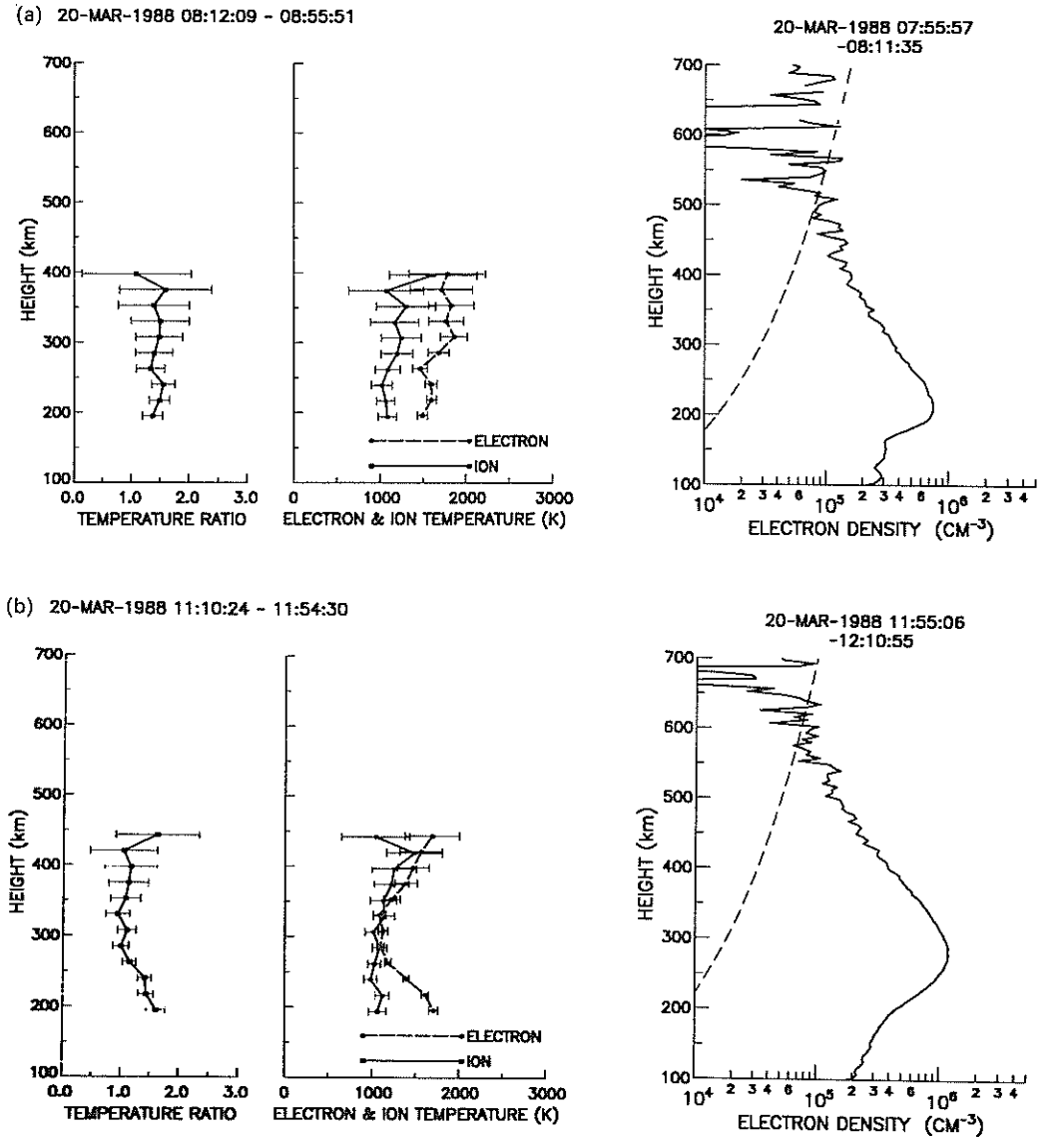
(a) 20-MAR-1988 08:12:09 - 08:55:51
HEIGHT (km)
TEMPERATURE RATIO
ELECTRON & ION TEMPERATURE (K)
ELECTRON
ION
20-MAR-1988 07:55:57
-08:11:35
ELECTRON DENSITY (CM^{-3})
(b) 20-MAR-1988 11:10:24 - 11:54:30
20-MAR-1988 11:55:06
-12:10:55

Fig. 12 (a) and (b).

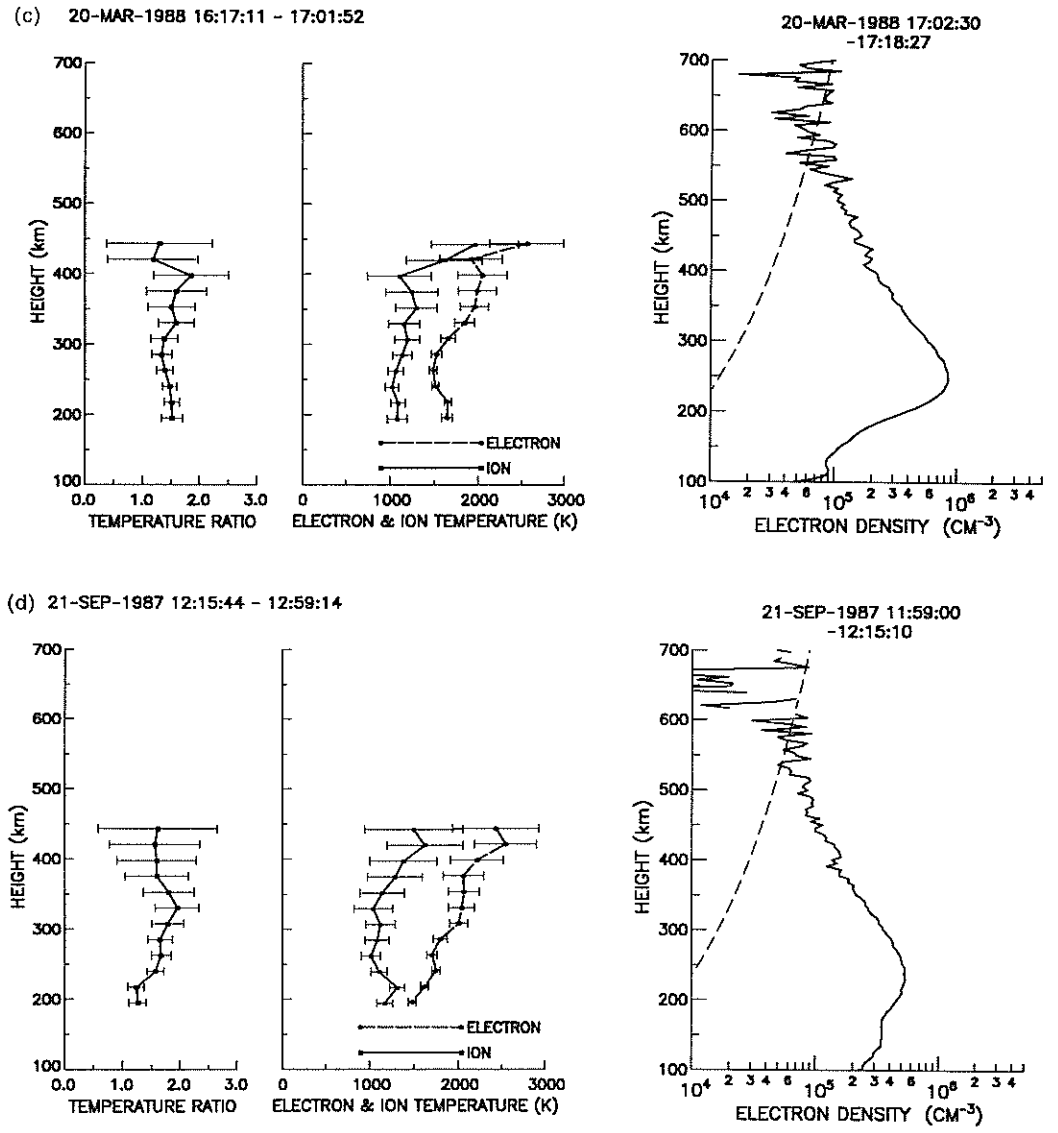

Fig. 12. Altitude profile measurements of N_e, T_e, T_i, and $T_r = T_e/T_i$ for four different periods: (a) 20 March 1988 at 8–9 LT, (b) 20 March 1988 at 11–12 LT, (c) 20 March 1988 at 16–17 LT, (d) 21 September 1987 at 12–13 LT.

Acknowledgements—One of us (WLO) was supported for this work through grant number INT89-03050 from the National Science Foundation of the United States under a co-operative agreement with the Japan Society for the Promotion of Science, and also under NSF grant ATM89-00042. The MU radar belongs to and is operated by the Radio Atmospheric Science Center of Kyoto University.

REFERENCES

BABCOCK R. B. JR and EVANS J. V.	1979	*J. geophys. Res.* **84,** 7348.
EVANS J. V.	1971	*Radio Sci.* **6,** 609.
FUKAO S., SATO T., TSUDA T., KATO S., WAKASUGI K. and MAKIHARA T.	1985a	*Radio Sci.* **20,** 1155.
FUKAO S., TSUDA T., SATO T., KATO S., WAKASUGI K. and MAKIHARA T.	1985b	*Radio Sci.* **20,** 1169.
KOHL H. and KING J. W.	1967	*J. atmos. terr. Phys.* **29,** 1045.
OLIVER W. L., FUKAO S., SATO T., TSUDA T., KATO S., KIMURA I., ITO A., SARYO T. and ARAKI T.	1988a	*J. Geomag. Geoelectr.* **40,** 963.
OLIVER W. L., FUKAO S., SATO T., TSUDA T., KATO S., KIMURA I., ITO A., SARYO T. and ARAKI T.	1988b	*J. geophys. Res.* **93,** 14649.
RICHMOND A. D., BLANC M., EMERY B. A., WAND R. H., FEJER B. J., WOODMAN R. F., GANGULY S., AMAYENC P., BEHNKE R. A., CALDERON C. and EVANS J. V.	1980	*J. geophys. Res.* **85,** 4658.
RICHMOND A. D., MATSUSHITA A. and TARPLEY J. D.	1976	*J. geophys. Res.* **81,** 547.
SARYO T., TAKEDA M., ARAKI T., SATO T., TSUDA T., FUKAO S. and KATO S.	1989a	*J. Geomag. Geoelectr.* **41,** 597.
SARYO T., TAKEDA M., ARAKI T., SATO T., TSUDA T., FUKAO S. and KATO S.	1989b	*J. Geomag. Geoelectr.* **41,** 727.
SATO T., ITO A., OLIVER W. L., FUKAO S., TSUDA T., KATO S. and KIMURA I.	1989	*Radio Sci.* **24,** 85.
STROBEL D. F. and MCELROY M. B.	1970	*Planet. Space Sci.* **18,** 1181.
TANAKA T. and HIRAO K.	1972	*Rept. Ionos. Space Res. Japan* **26,** 216.